Hindawi
Mathematical Problems in Engineering
Volume 2018, Article ID 8450213, 15 pages
https://doi.org/10.1155/2018/8450213

Research Article

A Novel Energy Management Strategy for Series Hybrid Electric Rescue Vehicle

Pei Li, Jun Yan, Qunzhang Tu, Ming Pan, and Jinhong Xue

Field Engineering College, Army Engineering University of PLA, Nanjing 210007, China

Correspondence should be addressed to Qunzhang Tu; tqzlhnj@126.com

Received 3 April 2018; Revised 26 July 2018; Accepted 27 August 2018; Published 29 October 2018

Academic Editor: Francesco Braghin

The performance and fuel consumption of hybrid electric vehicle heavily depend on the EMS (energy management strategy). This paper presents a novel EMS for a series hybrid electric rescue vehicle. Firstly, considering the working characteristics of engine and battery, the EMS combining logic threshold and fuzzy control is proposed. Secondly, a fuzzy control optimization method based on IQGA (improved quantum genetic algorithm) is designed to achieve better fuel efficiency. Then, the modeling and simulation are completed by using MATLAB/Simulink; the results demonstrate that the fuel consumption can be decreased by 5.17% after IQGA optimization and that the optimization effect of IQGA is better than that of GA (genetic algorithm) and QGA (quantum genetic algorithm). Finally, the HILS (hardware in loop simulation) platform is constructed with dSPACE; the HILS experiment shows that the proposed EMS can effectively improve the vehicle working efficiency, which can be applied to practical application.

1. Introduction

In recent years, natural disasters (such as earthquakes, debris flow, and heavy snowfall) have often occurred, causing inestimable loss to the people's life and property. As an important part of the emergency response system, rescue vehicles have a direct impact on the efficiency of disaster relief operations. The application of hybrid electric technology to rescue vehicles has aroused people's attention, by which the vehicle mobility and fuel efficiency can be significantly improved. At the same time, the generator can be used to provide power for lighting equipment, rescue equipment, and other electrical equipment, so the vehicle adaptability in harsh environment can be enhanced. However, the EMS plays a key role in the performance of hybrid electric system [1], which can be roughly classified into the following three categories.

(1) Logic Threshold Control Strategy. This strategy, which is widely used in many automobile enterprises, is simple and easy to develop, mainly including the "thermostat" control strategy and power following control strategy [2]. By setting the logic threshold to establish control rules, each power component can work in the high efficient area as much as possible. However, the setting of threshold value depends on the experiences of experts, and the optimal control effect cannot be guaranteed [3, 4].

(2) Optimization Based Control Strategy. By defining objective function, combining the constraint conditions, the control objective can be optimized by mathematical algorithm. This strategy can be subdivided into global optimization control strategy and instantaneous optimization control strategy. The former is designed based on given driving cycle, which is often used for vehicles with fixed routes, such as buses or commuter cars. Besides, it is also used as a criterion to evaluate other control strategies. Because the calculating quantity is large and complex, the optimization process cannot be carried out online. The representative strategies mainly include dynamic programming (DP) based strategy [5, 6], Pontryagin's minimum principle (PMP) based strategy [7, 8], Quadratic programming (QP) based strategy [9, 10], divide rectangle (DIRECT) algorithm based strategy [11–13], and convex optimization based strategy [14]. The latter is aimed at achieving optimal energy management in instantaneous state, which is not restricted by the specific driving cycle. The computation is relatively small and can be applied online,

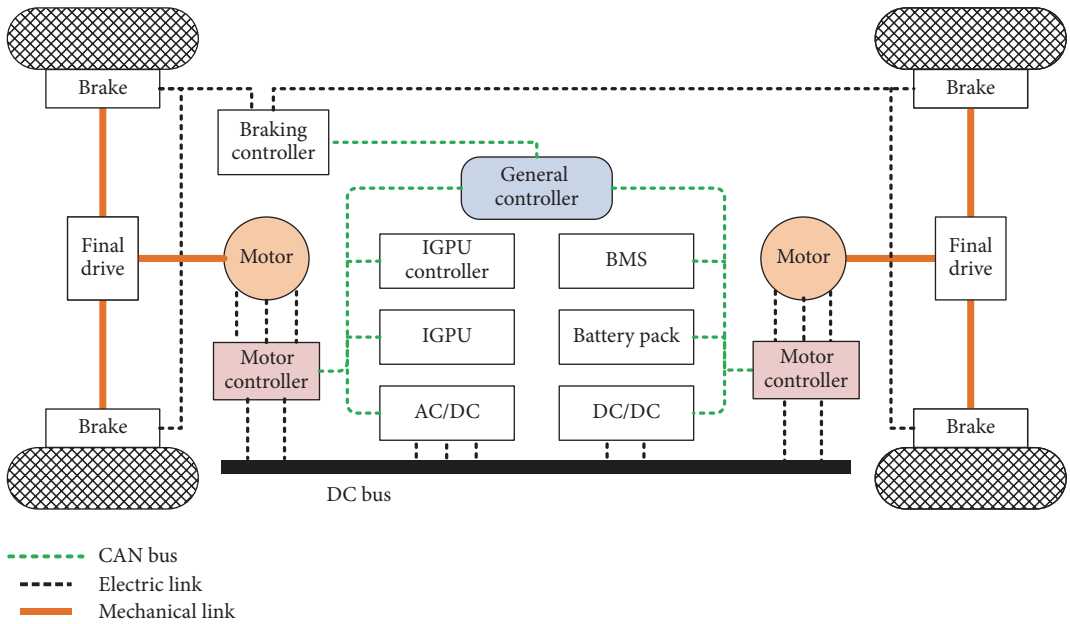

Figure 1: Structure diagram of the hybrid rescue vehicle.

such as fuel consumption minimization strategy (ECMS) [15–17] and model predictive control strategy (MPC) [18–20]. However, the instantaneous optimization belongs to local optimization, and the optimization effect depends on the precision of the mathematical model.

(3) Fuzzy Logic Control Strategy. With good real-time performance and robustness [21, 22], the fuzzy logic control strategy does not rely on precise mathematical models, which is suitable for dealing with the complex, nonlinear and time-varying problems. In practical applications, the speed, SOC, required torque, and power are often used as input variables [23–25], and the power ratio of the engine and the battery is used as the output variable. However, the formulation of control logic is mainly based on engineering experience, and it is difficult to ensure the optimal power distribution. To achieve better performance, many strategies combining fuzzy control method with other control methods have been proposed by some scholars. In [26], a fuzzy controller was used to adjust the equivalent factors of ECMS, and the fuel economy of the hybrid electric heavy-duty vehicle was improved. In [27], the DP algorithm was used to optimize the performance of ISG hybrid electric vehicle, and combined with the optimization results, a more practical fuzzy controller was proposed. In [28–30], some intelligent algorithms, such as genetic algorithm and particle swarm optimization, were used to optimize the membership function or control rules of the fuzzy controller. In [31–33], the mixed-fuzzy control strategy was designed by using neural network, working condition identification, machine learning, and other intelligent techniques. However, the control effects of the above strategies still exist a certain improvement space.

Considering the advantages and disadvantages of the above three categories of methods, a novel EMS is proposed to improve the fuel economy of a series hybrid electric rescue vehicle in this paper. First, combined with threshold control and fuzzy control, the EMS is initially designed according the working characteristics of engine and battery. Then, an improved quantum genetic algorithm with better convergence performance is proposed and applied to optimal the fuzzy controller. The structure of the paper is as follows: in Section 2, the configuration of a series hybrid electric rescue vehicle is introduced; in Section 3, the EMS of the whole vehicle is studied; in Section 4, the method for optimizing fuzzy control based on IQGA is designed; in Section 5, the offline simulation and HILS experiment are described; finally, the paper is concluded in Section 6.

2. Configuration of the Series Hybrid Electric Rescue Vehicle

In series hybrid electric system, there is no mechanical connection between the engine and the driving wheels, the speed, and torque of the engine can be controlled to any operating point on its speed-torque map. So by optimizing control, the fuel consumption and emission of the engine can be improved. As shown in Figure 1, the four-wheel drive structure with two motors is adopted to the rescue vehicle in this paper, which can not only increase the vehicle power performance, but also provide better regenerative braking effect. The electric drive system mainly includes general controller, internal-combustion-engine-generator power unit (IGPU) and its controller, battery pack and its management system (BMS), motors and motor controllers, rectifier, and DC/DC converter. The general controller is the core component, which is used to coordinate the power distribution of IGPU and battery pack according to the driver instruction, vehicle

Table 1: Specific parameters of the hybrid rescue vehicle.

Name	Value
Vehicle mass	14000kg
Frontal area	6.25m^2
Final drive ratio	7.9
Wheel radius	0.72m
Gravity center height	1672mm
Distance from gravity center to front wheel	3164mm
Wheel base	5200mm
Peak power of IGPU	260KW
Peak power of motor	150KW
Peak torque of motor	2400Nm
Battery capacity	92kWh

running state and other feedback information. As an auxiliary energy source, the battery pack provides additional power when the IGPU output power is insufficient, such as the situation of vehicle uphill and acceleration. The two motors can be used not only to provide driving force, but also to work as a generator to charge the battery when the vehicle is braking. The specific parameters of the vehicle are shown in Table 1.

3. Energy Management Strategy Design

Under the condition of satisfying vehicle power performance, how to coordinate the energy distribution between IGPU and battery to realize the optimization of vehicle efficiency is a primary problem that needed to be resolved for EMS. The following principles are taken into consideration in the formulation of EMS: (1) In order to improve engine efficiency, the minimum fuel consumption curve control method is adopted. (2) In order to make the battery not only able to provide power in time, but also able to recover the regenerative braking energy effectively, the battery SOC is controlled in the high efficiency area, and a certain margin is reserved for charging. (3) On the premise of braking stability, in order to make maximum use of the two motors to recover braking energy, the braking force distribution method based on I curve is adopted.

Through the experiments, the IGPU fuel consumption characteristics and battery internal resistance characteristics are obtained as shown in Figures 2 and 3, respectively. It is known that, when the IGPU output power is less than 50KW, the fuel economy is bad, and when SOC is in the range of 0.5~0.9, the battery working efficiency is high. Therefore, the IGPU output power is controlled within the range of 50~260KW, and the battery SOC is controlled within the range of 0.5~0.8 (SOC_{low}=0.5, SOC_{high}=0.8). According to the driving mode switch, battery SOC and required power, the vehicle working state is divided into four operating modes: pure electric traction mode, IGPU traction mode, hybrid traction mode, and braking mode. Each mode switches by the set threshold, and the flowchart of the EMS is shown in Figure 4.

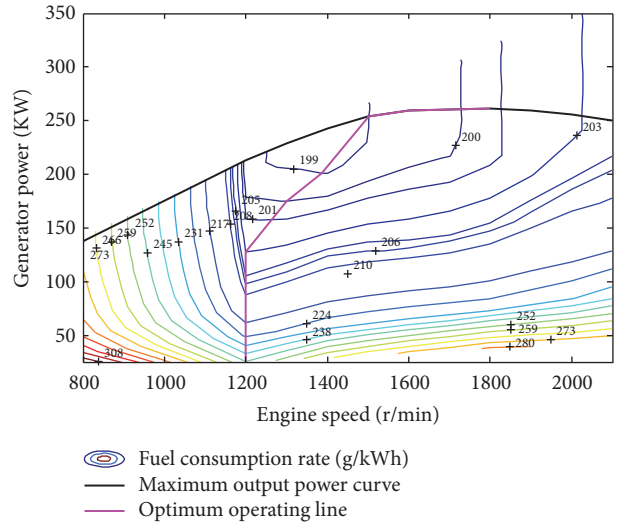

Figure 2: MAP of the IGPU.

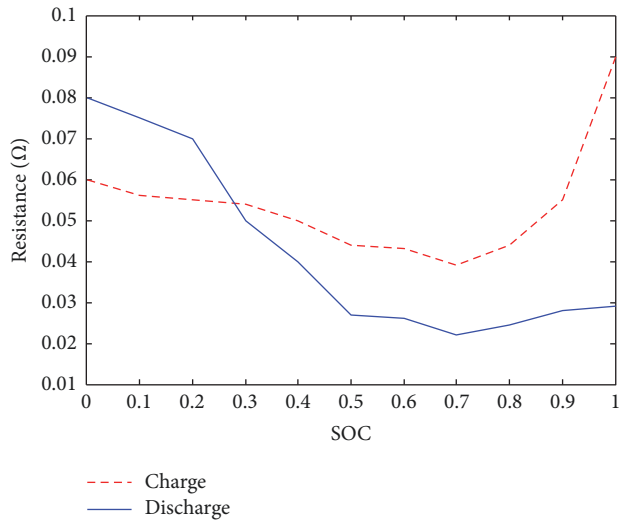

Figure 3: Battery internal resistance characteristics.

P_{req} is the required power of two motors, P'_g is the target power of IGPU, P'_b is the target power of battery, and P'_R is the target power of brake resistance. Define P_{cmax} is the maximum charging power of battery, and P_{dmax} is the maximum discharge power of battery. Assume that the charging current and power of the battery are negative and that the discharge current and power of the battery are positive; the energy distribution of different modes is as follows.

3.1. Pure Electric Traction Mode. In this mode, the battery alone supplies its power to meet the power demand. And this mode includes two cases (module 1 and module 2 in Figure 4): when the pure electric switch is opened, the vehicle is in pure electric drive mode A; when $0 \le P_{req} \le 50$KW and SOC $>$ SOC_{low}, the vehicle is in pure electric drive mode

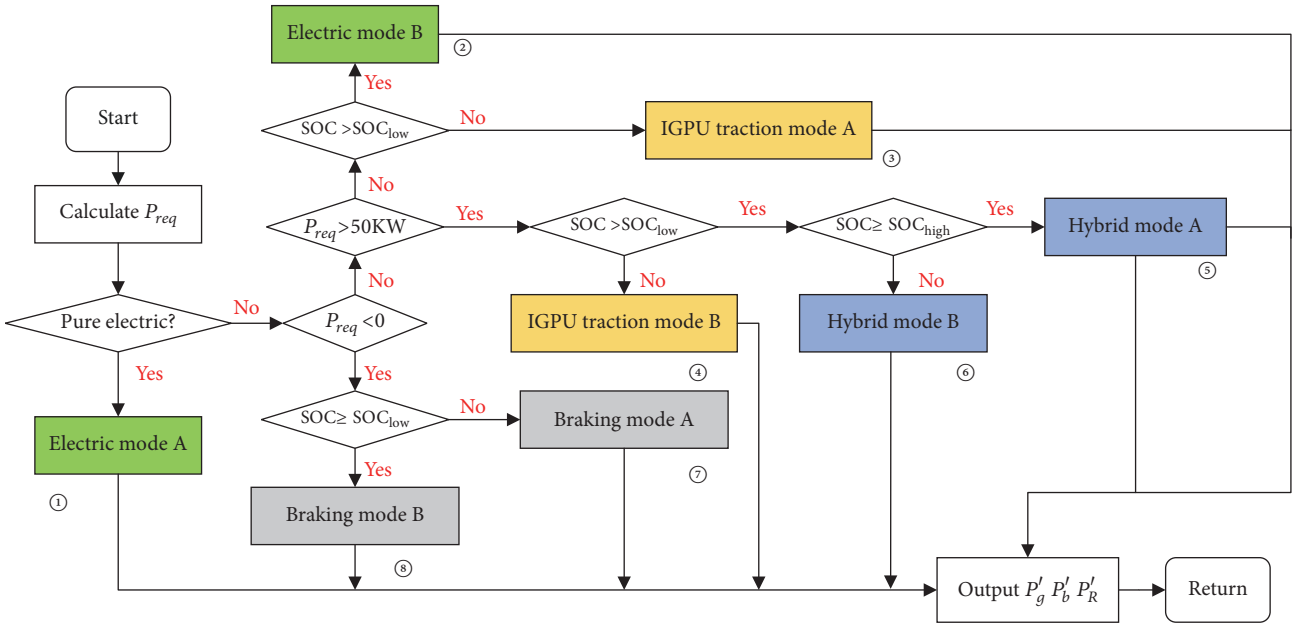

Figure 4: Flowchart of the EMS.

B. Both of these two cases are satisfied with the following formula:

$$P'_b = \min\left(P_{req}, P_{dmax}\right)$$
$$P'_g = 0 \tag{1}$$

3.2. IGPU Traction Mode. In this mode, IGPU not only provides power to propel the vehicle, but also provides power to charge the battery. There are also two cases included in this mode (module 3 and module 4 in Figure 4). When $0 \le P_{req} \le$ 50KW and SOC $\le$ SOC_{low}, the vehicle is in IGPU traction mode A, and the battery is charged with the maximum charging current:

$$P'_b = P_{cmax}$$
$$P'_g = P_{req} - P'_b \tag{2}$$

When P_{req} >50KW and SOC≤ SOC_{low}, the vehicle is in IGPU traction mode B:

$$P'_b = \max\left(P_{cmax}, P_{req} - 260\right)$$
$$P'_g = P_{req} - P'_b \tag{3}$$

3.3. Hybrid Traction Mode. This mode is also divided into two cases (module 5 and module 6 in Figure 4). When P_{req} >50KW and SOC≥ SOC_{high}, the vehicle is in hybrid traction mode A, at this time, the required power is mainly supplied by the battery, and the additional power is supplemented by IGPU; that is,

$$P'_b = \min\left(P_{req}, P_{dmax}\right)$$
$$P'_g = P_{req} - P'_b \tag{4}$$

When P_{req} >50KW and SOC_{low} < SOC < SOC_{high}, the vehicle is in hybrid traction mode B. Considering the efficiency of battery and the fuel economy of engine, the power distribution between the battery and IGPU is carried out by a Mamdani fuzzy logic controller (FLC) with double inputs and single output. The IGPU load coefficient λ ($\lambda = P_{req}/260$) and battery SOC are selected as input variables, power distribution coefficient k_g is selected as output variable. The target power of the battery and IGPU can be expressed as

$$P'_b = \left(1 - k_g\right) \cdot P_{req}$$
$$P'_g = k_g \cdot P_{req} \tag{5}$$

The relative membership function diagram is shown in Figure 5. λ, SOC, and k_g all have five fuzzy subsets: *VS*, *MS*, *M*, *MB*, *VB*, and the basic domain of λ, SOC, and k_g, respectively, are [0.1, 1.2], [0.5, 0.8], and [0.7, 1.5]. In the design process of FLC, the following principles should be noted: When λ is small, k_g should be raised so as to make the engine operate in its optimal operation region. When λ is large, k_g should be reduced so that the battery can supplement the additional power. When SOC is large or small, k_g should be reduced or raised so that the battery can be discharged or charged in time to keep SOC in the area with high efficiency. By using the rule form of "if λ is *A*, and SOC is *B*, then k_g is *C*", 25 fuzzy rules are established as shown in Table 2.

3.4. Braking Mode. Under driving mode, P_{req} can be calculated according to the angular displacement of accelerator pedal. However, for braking mode, P_{req} cannot be calculated by using the angular displacement of brake pedal, because the electrical regenerative braking coexists with mechanical braking. In this paper, the braking force of the motors is

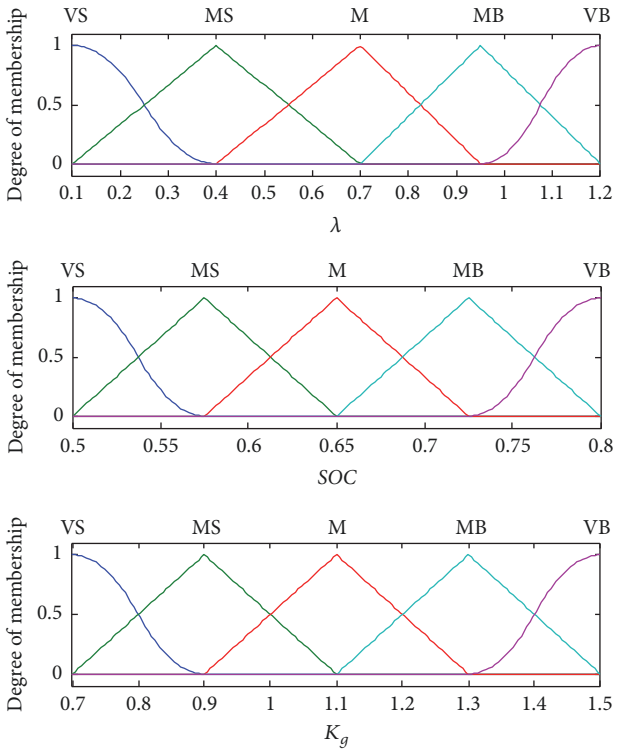

Figure 5: Membership function of the FLC.

Table 2: Fuzzy control rules.

λ	SOC				
	VS	MS	M	MB	VB
VS	VB	VB	MS	MS	MS
MS	VB	MB	MS	MS	VS
M	MB	MB	M	MS	VS
MB	MB	M	M	MS	VS
VB	MS	VS	VS	VS	VS

calculated by using of I curve, and then P_{req} is obtained combining with the vehicle speed. I curve is an ideal braking force distribution curve, as shown in Figure 6, where j is the deceleration of the vehicle during braking. Under this condition, the front axle braking force $F_{\mu 1}$ and rear axle braking force $F_{\mu 2}$ are satisfied with the following formula:

$$F_{\mu 2} = \frac{1}{2}\left[\frac{G}{h_g}\sqrt{b^2 + \frac{4h_g L}{G}F_{\mu 1}} - \left(\frac{Gb}{h_g} + 2F_{\mu 1}\right)\right] \quad (6)$$

where G is the vehicle gravity, h_g is the height of vehicle centroid, b is the distance between vehicle centroid and rear axle, and L is the wheelbase.

Besides, the sum of $F_{\mu 1}$ and $F_{\mu 2}$ is equal to the overall braking force; that is,

$$\beta \cdot F_{bra\_\max} = F_{\mu 1} + F_{\mu 2} \quad (7)$$

where β is conversion coefficient of brake pedal angle displacement ($\beta \in [-1, 0]$) and $F_{bra\_\max}$ is the maximum

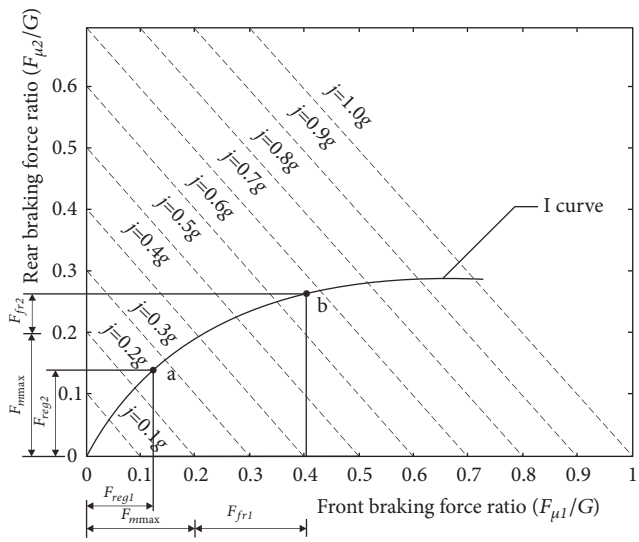

Figure 6: Ideal braking force distribution curve.

braking force of the vehicle. Combining formula (6) and formula (7), $F_{\mu 1}$ and $F_{\mu 2}$ can be obtained. $F_{\mu 1}$ and $F_{\mu 2}$ are usually composed of mechanical braking force and regenerative braking force. For more energy recapture, the regenerative braking should be given priority. If $F_{\mu 1}$ ($F_{\mu 2}$) is smaller than the maximum regenerative braking force of motor, the total braking force is provided by the motor and the mechanical brake is not used, as shown by point a in Figure 6. If $F_{\mu 1}$ ($F_{\mu 2}$) is greater than the maximum regenerative braking force of motor, the motor is controlled to produce the maximum regenerative braking force and the remaining force F_{fr1} (F_{fr2}) is provided by mechanical brake as shown by point b in Figure 6; that is,

$$\begin{aligned} F_{reg1} &= -\min\left(F_{\mu 1}, F_{m\max}\right) \\ F_{reg2} &= -\min\left(F_{\mu 2}, F_{m\max}\right) \end{aligned} \quad (8)$$

where F_{reg1}, F_{reg2} are the target regenerative braking force on the front axle and rear axle, respectively. $F_{m\max}$ is the maximum regenerative force of motor, and its value is limited by the motor speed N. In addition, it should be noted that the regenerative braking is affected by braking strength Z, vehicle speed V, and battery SOC.

When 0<Z<0.7, the motor can be controlled for regenerative braking. When Z≥0.7, the vehicle is in an emergency braking state. Considering braking safety, the motor should not work, and the mechanical brake has to produce the total braking force as required. The braking strength correction factor k_1 is introduced as

$$k_1 = \begin{cases} 1 & 0 \le Z < 0.7 \\ 0 & Z \ge 0.7 \end{cases} \quad (9)$$

When V≤12km/h, it is hard for the motors to produce brake torque due to the low speed. Therefore, with the vehicle speed drops to 12 km/h, the regenerative braking force should

be gently reduced to 0. The speed correction factor k_2 is introduced as

$$k_2 = \begin{cases} 1 & V > 24 \\ \frac{1}{12}V - 1 & 12 < V \le 24 \\ 0 & \end{cases} \tag{10}$$

When the value of SOC is very high (SOC>0.99), the battery will be damaged if it is still charged. Therefore, with the battery SOC up to 0.99, the regenerative braking force should also be gently reduced to 0. The SOC correction factor k_3 is introduced as

$$k_3 = \begin{cases} 1 & \text{SOC} < 0.8 \\ -6.667\text{SOC} + 6.333 & 0.8 \le \text{SOC} < 0.99 \\ 0 & \text{SOC} \ge 0.99 \end{cases} \tag{11}$$

The actual regenerative braking force on the front axle and rear axle F'_{reg1} and F'_{reg2} can be expressed as

$$\begin{aligned} F'_{reg1} &= k_1 \cdot k_2 \cdot k_3 \cdot F_{reg1} \\ F'_{reg2} &= k_1 \cdot k_2 \cdot k_3 \cdot F_{reg2} \end{aligned} \tag{12}$$

Therefore, the P_{req} under braking state can be expressed as

$$P_{req} = \frac{\left(F'_{reg1} + F'_{reg2}\right) \cdot r}{i_0} \cdot N \tag{13}$$

where r is wheel radius and i_0 is final drive ratio. The braking state can be divided into two cases according to SOC value (module 7 and module 8 in Figure 4). When SOC< SOC_{low}, the vehicle is in braking mode A. The battery should be charged with maximum current, and the brake resistance does not work; that is,

$$\begin{aligned} P'_b &= -\min\left(\left|P_{\text{cmax}}\right|, P_{g\text{max}} - K_{bra}P_{req}\right) \\ P'_g &= -K_{bra}P_{req} - P'_b \\ P'_R &= 0 \end{aligned} \tag{14}$$

where K_{bra} is the maximum regenerative braking coefficient. When SOC≥ SOC_{low}, the vehicle is in braking mode B. The battery is charged normally and IPGU does not work. If the recovery energy is too much, the excess energy can be consumed in the form of thermal energy by using the brake resistance; that is,

$$\begin{aligned} P'_b &= -\min\left(\left|P_{\text{cmax}}\right|, -K_{bra}P_{req}\right) \\ P'_g &= 0 \\ P'_R &= K_{bra}P_{req} - P'_b \end{aligned} \tag{15}$$

4. Implementation of the IQGA for FLC

Because the FLC design is mainly based on the engineering experiences of experts, there is room for improvement. In this section, in order to improve the fuel economy of hybrid power system, the IQGA is proposed to optimize the fuzzy control strategy.

4.1. Improved Quantum Genetic Algorithm. The quantum genetic algorithm (QGA) is a probability search algorithm based on the theory of quantum computing, which is proposed by Han [34]. In QGA, quantum state vector is used for genetic encoding, and qubit rotation gate is used to realize chromosome evolution. Therefore, the algorithm has strong parallelism, which can achieve better calculation results than conventional genetic algorithm (GA). However, its convergence performance leaves room to improve. The IQGA is proposed in this paper based on the improvement of QGA. The dynamic adjusting rotation gate is adopted to improve the convergence speed, and quantum catastrophic operation is introduced to overcome premature convergence and improve global optimization ability.

4.1.1. Qubit Encode. A qubit can be interpreted not only "0" state or "1" state, but also any superposition of them. It can be expressed as

$$\left|\varphi\right\rangle = \alpha\left|0\right\rangle + \beta\left|1\right\rangle \tag{16}$$

where α and β are complex numbers, satisfying $|\alpha|^2 + |\beta|^2 = 1$. $|\alpha|^2$ and $|\beta|^2$ represent the probability of qubit in 0 state and 1 state, respectively. The multiqubits can be used to represent the chromosome with multigenes, as follows:

$$q_j^t = \begin{bmatrix} \alpha_{11}^t & \left|\alpha_{12}^t\right| & \cdots & \left|\alpha_{1k}^t\right| & \alpha_{21}^t & \left|\alpha_{22}^t\right| & \cdots & \left|\alpha_{2k}^t\right| & \cdots & \left|\alpha_{m1}^t\right| & \alpha_{m2}^t & \left|\cdots\right| & \alpha_{mk}^t \\ \beta_{11}^t & \left|\beta_{12}^t\right| & \cdots & \left|\beta_{1k}^t\right| & \beta_{21}^t & \left|\beta_{22}^t\right| & \cdots & \left|\beta_{2k}^t\right| & \cdots & \left|\beta_{m1}^t\right| & \beta_{m2}^t & \left|\cdots\right| & \beta_{mk}^t \end{bmatrix} \tag{17}$$

where q_j^t is the j-th individual chromosome in t-th generation, k is the number of qubits used for each gene encoding, and m is the number of genes in the chromosome.

4.1.2. Measure. The measuring method for the t-th generation population $Q(t) = (q_1^t, q_2^t, \ldots, q_n^t)$ is as follows: For each qubit, generate a random number N_{rand} between 0 and 1; if $\text{N}_{\text{rand}} \le |\alpha|^2$, the qubit is 0; otherwise 1. Then the binary

Table 3: Look-up table of function $f(\alpha_i, \beta_i)$.

b_i	$Best_i$	$f(x_i) > f(Best)$	$\Delta\theta_i$	$f(\alpha_i, \beta_i)$			
				$\alpha_i \cdot \beta_i > 0$	$\alpha_i \cdot \beta_i < 0$	$\alpha_i = 0$	$\beta_i = 0$
0	0	False	0	0	0	0	0
0	0	True	0	0	0	0	0
0	1	False	δ	1	-1	0	±1
0	1	True	δ	-1	1	±1	0
1	0	False	δ	-1	1	±1	0
1	0	True	δ	1	-1	0	±1
1	1	False	0	0	0	0	0
1	1	True	0	0	0	0	0

coding population $P(t) = (x_1^t, x_2^t, \ldots, x_n^t)$ can be obtained. Suppose X_m represents the decimal value corresponding to the m-th gene $x_m = (b_k b_{k-1} \cdots b_2 b_1)$, which is in the range between $U_m^{\max}$ and $U_m^{\min}$; x_m can be converted to X_m as follows:

$$X_m = U_m^{\min} + \left(\sum_{i=1}^{k} b_i \cdot 2^{i-1} \right) \cdot \frac{U_m^{\max} - U_m^{\min}}{2^k - 1} \tag{18}$$

Then the decimal measurement value of the nth chromosome $X_n^t = (X_1, X_2, \cdots, X_m)$ can be calculated. By the same method, the decimal value of the t-th generation population $S(t) = (X_1^t, X_2^t, \cdots, X_n^t)$ is obtained.

4.1.3. Qubit Rotation Gate Strategy. The quantum rotation gate $U(\theta)$ is the executing mechanism of updating operation, which directly affects the algorithm performance. It can be expressed as

$$U(\theta) = \begin{bmatrix} \cos(\theta) & -\sin(\theta) \\ \sin(\theta) & \cos(\theta) \end{bmatrix} \tag{19}$$

The updating operation of qubit is as follows:

$$\begin{bmatrix} \alpha_i' \\ \beta_i' \end{bmatrix} = U(\theta) \begin{bmatrix} \alpha_i \\ \beta_i \end{bmatrix} = \begin{bmatrix} \alpha_i \cos(\theta) - \beta_i \sin(\theta) \\ \alpha_i \sin(\theta) + \beta_i \cos(\theta) \end{bmatrix} \tag{20}$$

where $(\alpha_i, \beta_i)^T$ and $(\alpha_i', \beta_i')^T$ are the probability amplitude of ith qubit before and after updating, respectively. θ is the rotation angle, in general, $\theta \in [0.001\pi, 0.05\pi]$, and it can be expressed as

$$\theta = \Delta\theta_i \cdot f(\alpha_i, \beta_i) \tag{21}$$

where $\Delta\theta_i$ and $f(\alpha_i, \beta_i)$ are the value and direction of the rotation angle, and they can be obtained by Table 3. In Table 3, b_i and $Best_i$, respectively, are the ith bit of the current measuring individual and optimal individual; $f(x_i)$ and $f(Best)$, respectively, are the fitness values of the current measuring individual and optimal individual. δ is a dynamic value, which is used to control the convergence speed of the algorithm; it can be expressed as

$$\delta = \theta_{\min} + \left(\frac{e^{(MAXGEN-t)/(MAXGEN-1)} - 1}{e - 1} \right) (\theta_{\max} - \theta_{\min}) \tag{22}$$

where t is the evolution generation, $MAXGEN$ is the largest evolution generation, and $\theta_{\max}$ and $\theta_{\min}$ are the maximum rotation angle and minimum rotation angle, respectively. δ is decreased with the increase of evolution generation, so as to realize the dynamic adaptive adjustment of the qubit rotation gate.

4.1.4. Population Catastrophe. After several generations of evolution, the algorithm may fall into the local optimal solution. The population catastrophe can be used to solve this problem. For each evolution, the average fitness of the population f_{avg} can be calculated as follows:

$$f_{avg} = \frac{\sum_{i=1}^{n} f_i}{n} \tag{23}$$

where f_i represents the fitness value of the ith individual and n is the number of individuals in the population. The fitness values which is greater than f_{avg} are averaged to get f_{avg}' and define the catastrophe factor Δf as

$$\Delta f = \left| f_{avg} - f_{avg}' \right| \tag{24}$$

If Δf is very small, it indicates that the diversity of the population is poor, and the catastrophe should be carried out at this time; that is, only the best individual is retained and the others should be regenerated.

4.2. FLC Optimization. The membership function is the key factor affecting the performance of FLC, so the decisive parameters of the membership function are optimized in this paper. Take λ as an example; as shown in Figure 7, the location of the vertexes of the red triangles A, B, and C determines the shape of the membership function. Therefore, the distance between the line segments AD, AE, and EC (i.e., x1, x2, and x3) can be used as the variables to be optimized. The number of variables can be reduced effectively by this method, which greatly reduces the computational complexity. The same coding method is used to optimize the membership function of SOC and k_g. Thus there are 9 variables to be optimized; that is, there are 9 genes in the chromosome.

During the driving cycle, both the battery and the engine-generator set need to provide energy for the vehicle. To eliminate the effect of battery energy on fuel consumption,

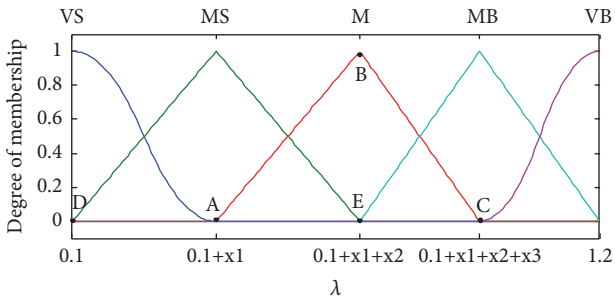

FIGURE 7: Optimized variables of λ.

the battery SOC of final state before and after optimization should be controlled at the same level. The ideal situation is that the final state SOC difference ΔSOC is controlled to 0, but in this case, the amount of calculation will become very large. In order to improve the speed of simulation, a certain tolerance of ΔSOC can be set. In this paper, the tolerance is 0.5% [35, 36]; that is, the constraint on SOC is defined as

$$-0.5\% \le \Delta \mathrm{SOC} \le 0.5\% \tag{25}$$

Under the condition of satisfying vehicle power performance, aiming at the goal of low fuel consumption in urban and high speed driving cycle, the objective function is obtained as follows [37]:

$$ObjFun = \frac{1}{0.55/City\_V_b + 0.45/Hwy\_V_b} \tag{26}$$

where $City\_V_b$ and Hwy_V_b are the engine fuel consumption (L) under the urban and high speed driving cycle, respectively.

The optimization process of the fuzzy controller based on IQGA is shown in Figure 8, and the specific steps are as follows:

(1) Initialize the population $Q(t_0)$; randomly generate n chromosomes encoded with qubits.

(2) Get the confirmed solution $S(t_0)$ by measuring $Q(t_0)$.

(3) Assign $S(t_0)$ to FLC, evaluate $Q(t_0)$, and record the optimal individual $q_{best}^{t_0}$ and its fitness $ObjFun_{beat}^{t_0}$.

(4) Decide whether the calculation process can be finished; if it meets the termination condition, end, or go on.

(5) Get the confirmed solution $S(t)$ by measuring $Q(t)$, assign $S(t)$ to FLC, evaluate $Q(t)$, and record the individual fitness $ObjFun_i^t$ $(i \in \{1, \ldots, n\})$ of $Q(t)$.

(6) Update $Q(t)$ by using quantum rotation gate $U(\theta)$ and population catastrophe; get new population $Q(t+1)$.

(7) Evaluate $Q(t+1)$; get the optimal individual q_{best}^t and its fitness $ObjFun_{beat}^t$.

(8) $t+1$, return to step (4).

5. Simulation and HILS Experiment

In this section, the effectiveness of the proposed EMS for series hybrid electric rescue vehicle is validated. Firstly, the simulation model of the vehicle is built with Simulink. Then, the offline optimization simulation is carried out. Finally,

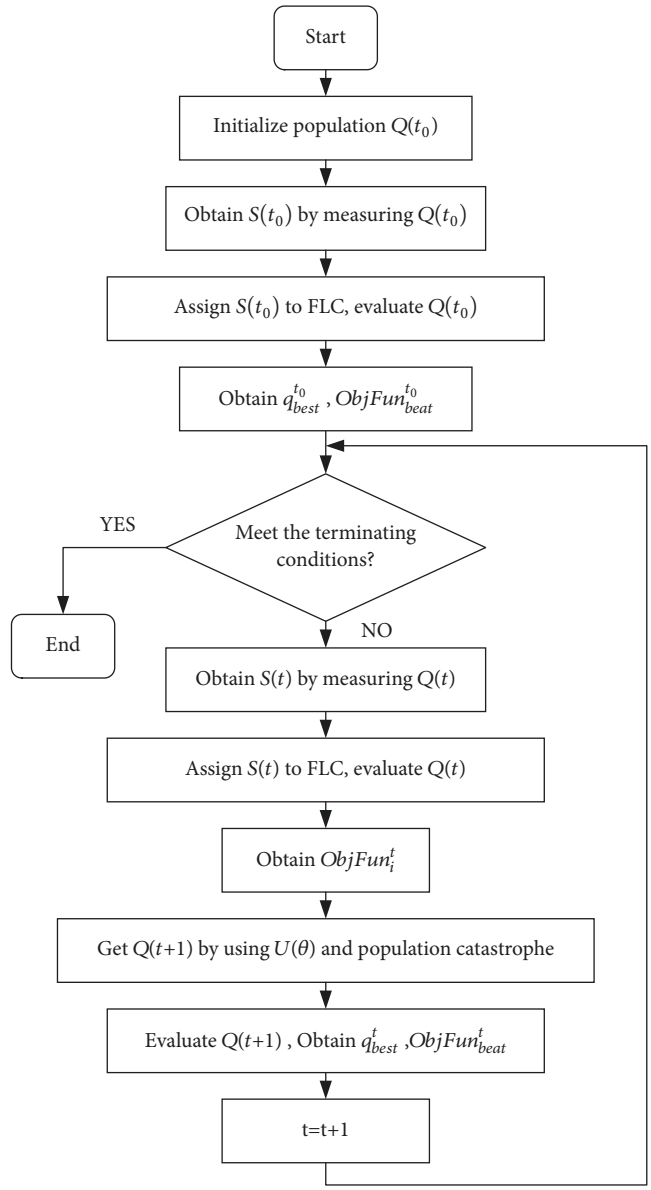

FIGURE 8: FLC optimization process based on IQGA.

using the DISPACE platform, the driver-controller based HILS platform is established with which to verify the real-time performance of the control strategy.

5.1. System Mathematical Models. The simulation model of series hybrid electric rescue vehicle, as shown in Figure 9, is mainly made up of driver model, drive torque distribution model, braking torque distribution model, vehicle dynamics model, control strategy model, driving mode judgment model, motor model, engine-generator model, DC/DC converter model, and battery model. The driver model is built based on PID control, and the error of target speed and actual speed is taken as the input [38]. The driving torque distribution model, braking torque distribution model, motor model, and control strategy model are built on the basis of the

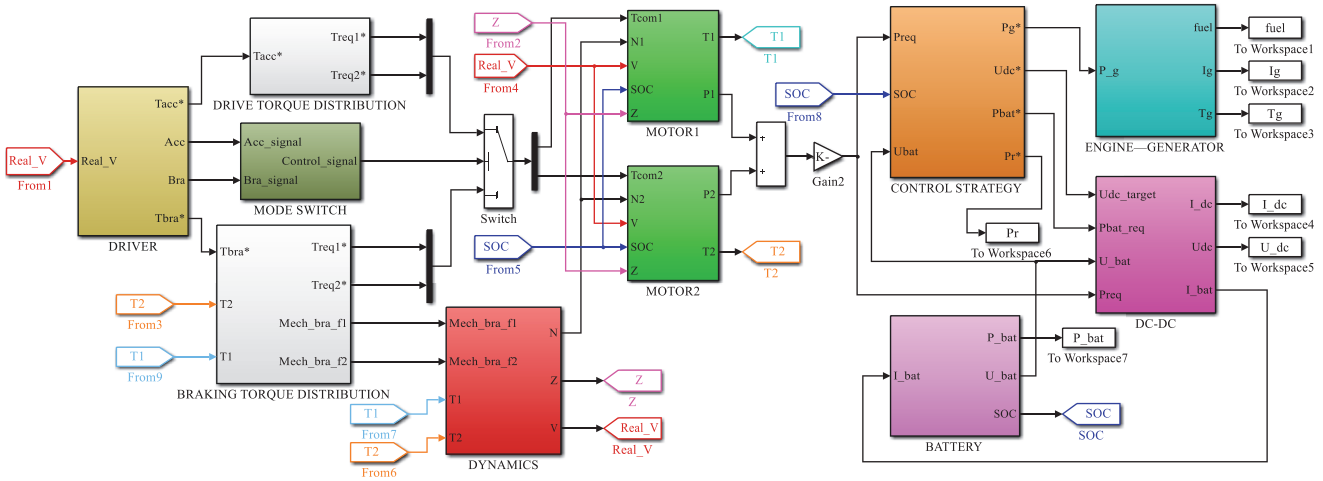

FIGURE 9: Simulation model of series hybrid electric rescue vehicle.

EMS proposed in Section 3. The following mainly introduces the vehicle dynamics model, engine-generator model, and battery model.

(1) Vehicle Dynamics Model. The vehicle dynamics model is built based on longitudinal dynamics characteristics of the vehicle; the torque of wheel T_w can be expressed as

$$T_w = i_0 \cdot (\eta_{T1} \cdot T_1 + \eta_{T2} \cdot T_2) - (T_{mech1} + T_{mech2}) \quad (27)$$

where η_{T1} and η_{T2} are the transmission efficiency of the front and rear motor, respectively. T_1 and T_2 are the output torque of the front and rear motor, respectively; T_{mech1} and T_{mech2} are the mechanical braking torque of the front and rear axle, respectively. T_w can also be expressed as

$$T_w = \left[mgC_r \cos\alpha + \frac{1}{2} C_D \rho A u^2 + mg \sin\alpha + \delta' m \frac{du}{dt} \right] \quad (28)$$

where m is the vehicle mass (kg), g is the gravity acceleration, C_r is the rolling resistance coefficient, α is the road-grade angle, C_D is the air drag coefficient, ρ is the air density, A is the frontal area of the vehicle (m^2), δ' is the correction coefficient of rotating mass, and u is the vehicle speed (m/s). The front and rear motor speed N_1 and N_2 (r/min) have the following relationship with u:

$$N_1 = N_2 = \frac{30 i_0 u}{\pi r} \quad (29)$$

(2) Engine-Generator Model. Because there is velocity coupling between the engine and generator, they are modeled as a whole. The equivalent circuit of engine-generator set is shown in Figure 10 [39]. Ignoring the internal resistance and torque loss, the DC bus voltage U_{dc} and the generator electromagnetic torque T_g can be expressed as

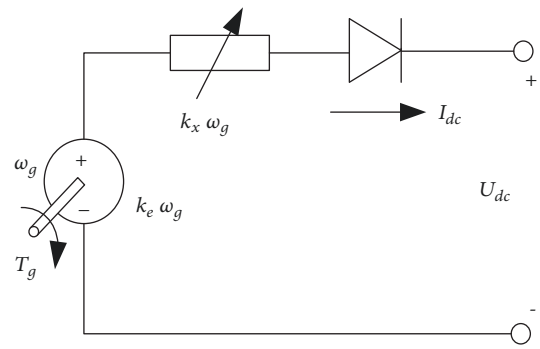

FIGURE 10: The equivalent circuit of engine-generator set.

$$U_{dc} = K_e \omega_g - K_x \omega_g I_{dc}$$
$$T_g = \frac{P_g'}{\omega_g} = K_e I_{dc} - K_e I_{dc}^2 \quad (30)$$

where K_e and K_x are the electromotive force coefficient and equivalent impedance coefficient of the generator, respectively, and they can be obtained from the bench test data. ω_g is the rotation angular velocity of generator; I_{dc} is the DC bus current. The engine and the generator are connected by a speed increase box, and the speed increasing ratio is i_{eg}. According to the torque balance, the following equations can be obtained:

$$\frac{T_{eng}}{i_{eg}} - T_g = 0.1047 \left(\frac{J_e}{i_{eg}^2} + J_g \right) \frac{dn_g}{dt}$$
$$n_g = i_{eg} n_{eng} \quad (31)$$

where T_{eng} is the engine torque and J_e and J_g are the moment of inertia of engine and generator, respectively. n_{eng} and n_g are the rotational speed of engine and generator,

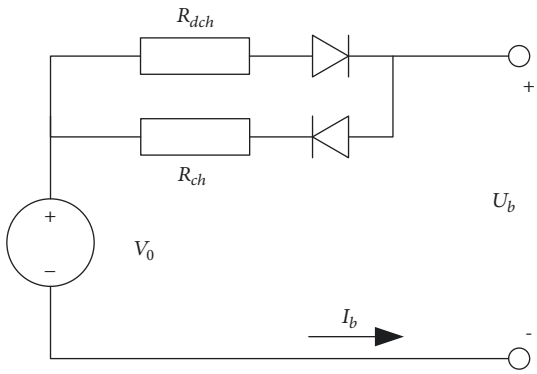

Figure 11: The equivalent circuit of battery.

respectively. In addition, the engine fuel consumption V_e can be calculated from formula (32):

$$V_e = \frac{b_e T_{eng} n_{eng}}{9550 \eta_e \rho_e} \tag{32}$$

where b_e is the fuel consumption rate ($b_e = f(T_{eng}, n_{eng})$), ρ_e is the fuel density, and η_e is the engine output efficiency.

(3) Battery Model. The battery model is built by using the typical Rint model [40], and the equivalent circuit is shown in Figure 11. U_b, V_0, I_b, R_{ch}, and R_{dch} are the terminal voltage, open-circuit voltage, internal current (positive when discharge), charge resistance, and discharge resistance of the battery, respectively. Among them, the values of V_0, R_{ch}, and R_{dch} are all related to the battery SOC, so the following equations can be obtained:

$$\begin{aligned} U_b &= V_0 - I_b R_{dch} \quad I_b > 0 \\ U_b &= V_0 - I_b R_{ch} \quad I_b < 0 \\ V_0 &= f_1(\mathrm{SOC}) \\ R_{dch} &= f_2(\mathrm{SOC}) \\ R_{ch} &= f_3(\mathrm{SOC}) \end{aligned} \tag{33}$$

The ampere hour method [41] is applied to estimate the battery SOC. Suppose the maximum capacity of the battery is $Q_{\max}$, and the initial capacity of the battery is Q_0, then the battery SOC at time t can be expressed as

$$SOC = \frac{Q_0 - \int_0^t I_b(t)\,dt}{Q_{\max}} \times 100\% \tag{34}$$

5.2. Simulation. The driving cycle used in the simulation, as shown in Figure 12, is mainly composed of UDDS urban driving cycle and HWFET high speed driving cycle. In order to compare the optimization effect of different algorithms, GA, QGA, and IQGA are used to optimize the FLC, respectively. Supposing that the genetic algebra is 200, that the population size is 50, and that the binary length of each variable is 10, the simulation is carried out by using MATLAB/Simulink. The

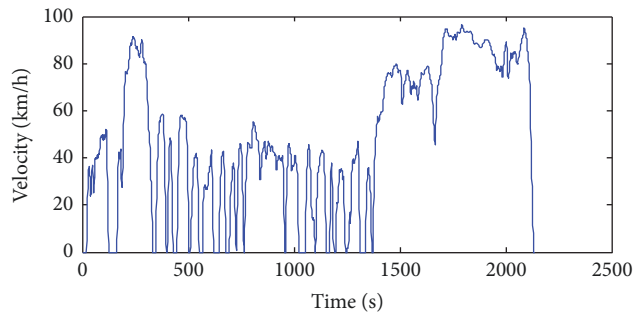

Figure 12: UDDS and HWFET combined driving cycle.

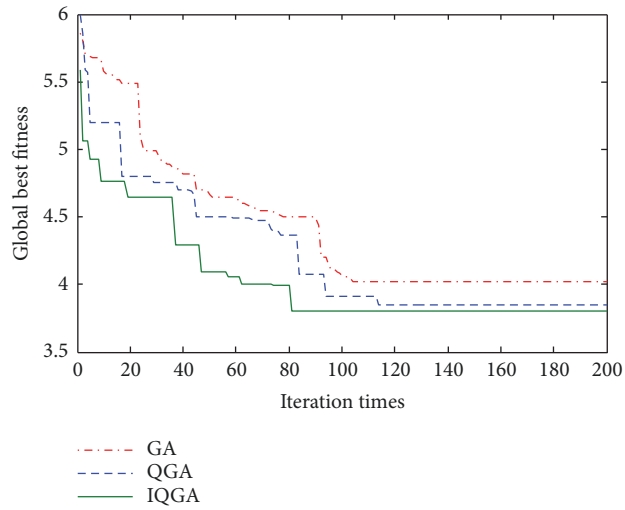

Figure 13: Optimization process of different algorithms.

changing curves of global fitness with different strategies are shown in Figure 13. It can be seen that, under the condition of same population size and generation, the fitness of IQGA reaches the minimum value 3.8 after 80 generations, while the fitness of QGA reaches the minimum value 3.85 after 114 generations and the fitness of GA reaches the minimum value 4.02 after the 104 generations. It shows that IQGA has faster convergence speed and better optimization result than QGA and GA, which is more suitable for solving the optimization problem of EMS. The fuzzy control membership function optimized by IQGA is shown in Figure 14.

Figures 15 and 16, respectively, reveal the distribution of IGPU operating points before and after IQGA optimization. It can be seen that, compared with the original fuzzy control strategy, the optimized IGPU operating points are more distributed in the high efficiency region. The changing curves of battery SOC before and after optimization are shown in Figure 17. It shows that the initial SOC value is 0.7; after IQGA optimization, the final SOC value changed from 0.677 to 0.674. It is observed that ΔSOC= -0.44%, which satisfies the SOC constraints set in (25). Figure 18 shows the fuel consumption before and after optimization. It can be seen that the fuel consumption is 8.71L before optimization, while it drops by 5.17% to 8.26L after optimization. Therefore, the results indicate that, with IQGA optimized control strategy,

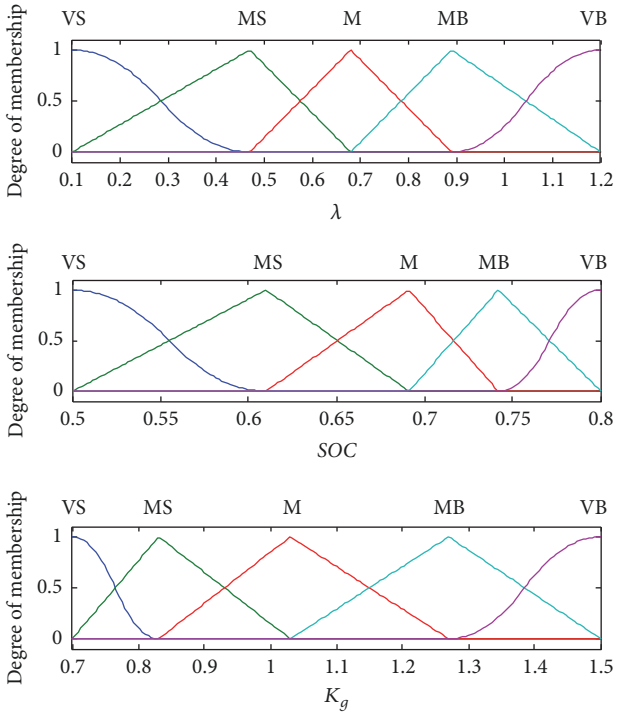

Figure 14: Membership function optimized by IQGA.

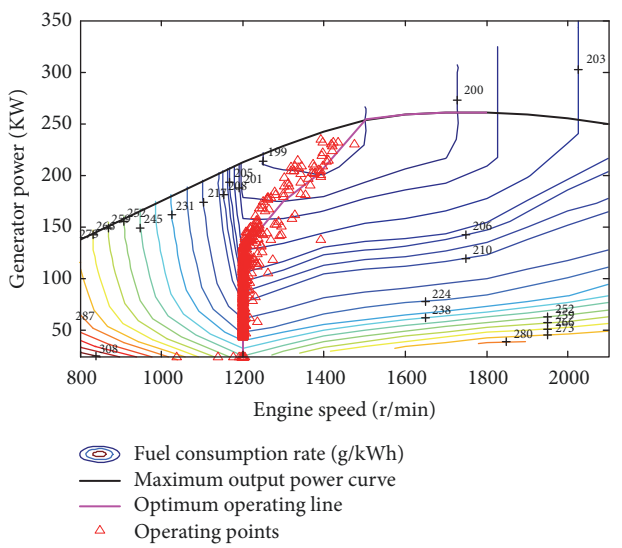

Figure 15: IGPU operating points before IQGA optimization.

the fuel consumption can be effectively reduced and the IGPU efficiency can be significantly improved.

5.3. HILS Experiment. In offline simulation, the driver's operation habits and the real-time operation effect of control strategy are not considered. In order to validate the proposed EMS in real-world implementation, the HILS experiment based on driver and controller is carried out with dSPACE.

Using dSPACE, the Simulink models could be converted into C codes and run reliably [42, 43]. The schematic diagram

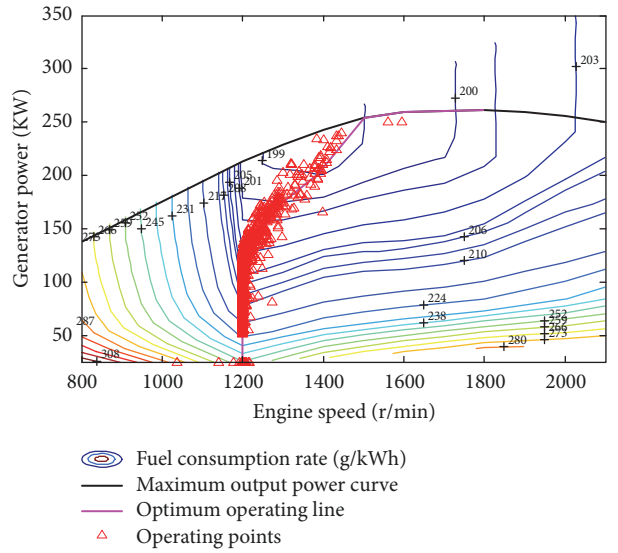

Figure 16: IGPU operating points after IQGA optimization.

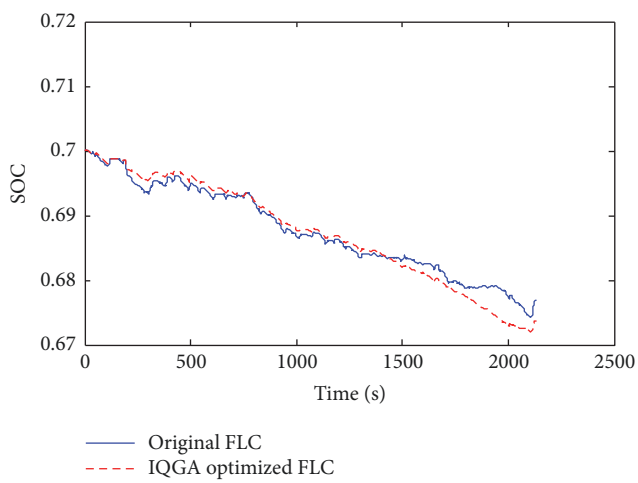

Figure 17: Changing curve of battery SOC.

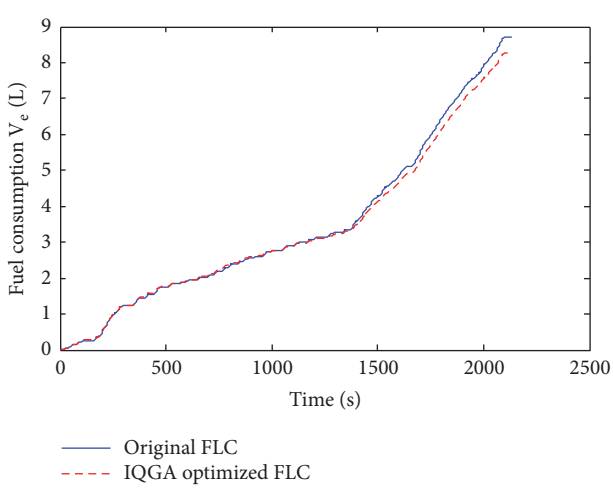

Figure 18: Fuel consumption.

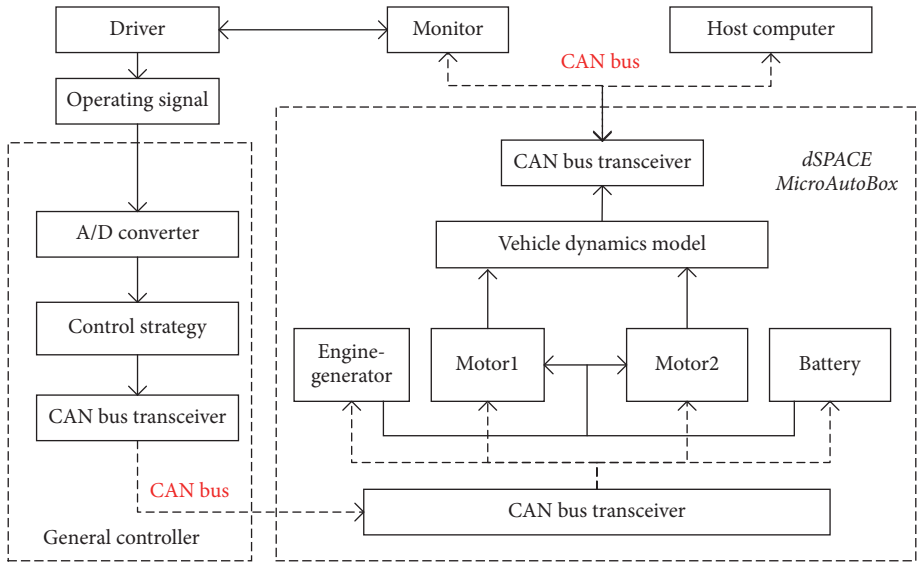

Figure 19: Schematic diagram of HILS platform.

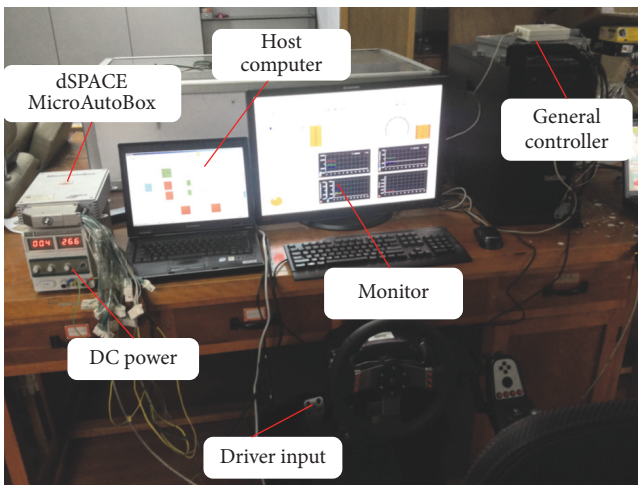

Figure 20: Hardware of HILS platform.

of HILS platform is shown in Figure 19. The driver controls the acceleration or brake pedal to produce analog signals which are transmitted to the general controller through the A/D interface. After calculation and analysis, the control signal produced by general controller is input to dSPACE through the CAN bus. According to the control instruction, the engine-generator model, battery model, motor model, and vehicle dynamics model are run in dSPACE. Meanwhile, the operating parameters are displayed on the monitor. The host computer is used to modify, compile, and download the internal models of dSPACE. The hardware of HILS platform is shown in Figure 20.

According to the driver's driving habits, the HILS experiment is carried out under a typical 70 seconds driving condition, and the results are shown in Figure 21. Figure 21(a) shows the driver's operation signal, and Figure 21(b) shows the vehicle speed. As we can see, in 1-11s, the vehicle experienced a slight acceleration, and the speed increased from 0 to 11 km/h. In 12-17s, the vehicle experienced a slight braking, and the speed fell to 2 km/h. In 18-33s, the vehicle experienced a medium strength acceleration, and the speed rose to 47 km/h. In 34-41s, the vehicle experienced a medium strength braking, and the speed fell to 14 km/h. In 42-62s, the vehicle experienced two types of quick acceleration, and the speed rose to 88 km/h. In 63-65s and 69-70s, the vehicle was in the state of gliding, and the speed decreased for the driving resistance. In 66-68s, the vehicle experienced an emergency braking, and the speed fell to 3 km/h. It can be seen that the vehicle speed curve is smooth and stable, which can follow the driver's acceleration or braking intention very well.

Figure 21(c) shows the motor demand power P_{req}, IGPU output power P_g, and battery output power P_b. It can be seen that the battery plays a good role in reducing peak and filling valley: when the demand power is negative, the energy can be recovered effectively; when the demand power is high, the compensation power can be output in time. Meanwhile, the engine works in the efficient area above 50KW, and when the demand power is small, it can be properly adjusted to output larger power to charge the battery.

In Figure 21(d), the torque distribution of the front and rear axle is shown. When the vehicle is driven, the driving torque on the front axle is the same with that of rear axle. When the vehicle is braking, the braking torque on the front and rear axle can be distributed according to the I curve.

Figures 21(e) and 21(f) show the distribution of mechanical torque and motor torque on front and rear axle, respectively. It can be seen that when the vehicle is driven, the motor torque can basically meet the demand torque, but when the vehicle speed is high, the motor torque is not sufficient enough for accelerating. When the vehicle is braking, it needs

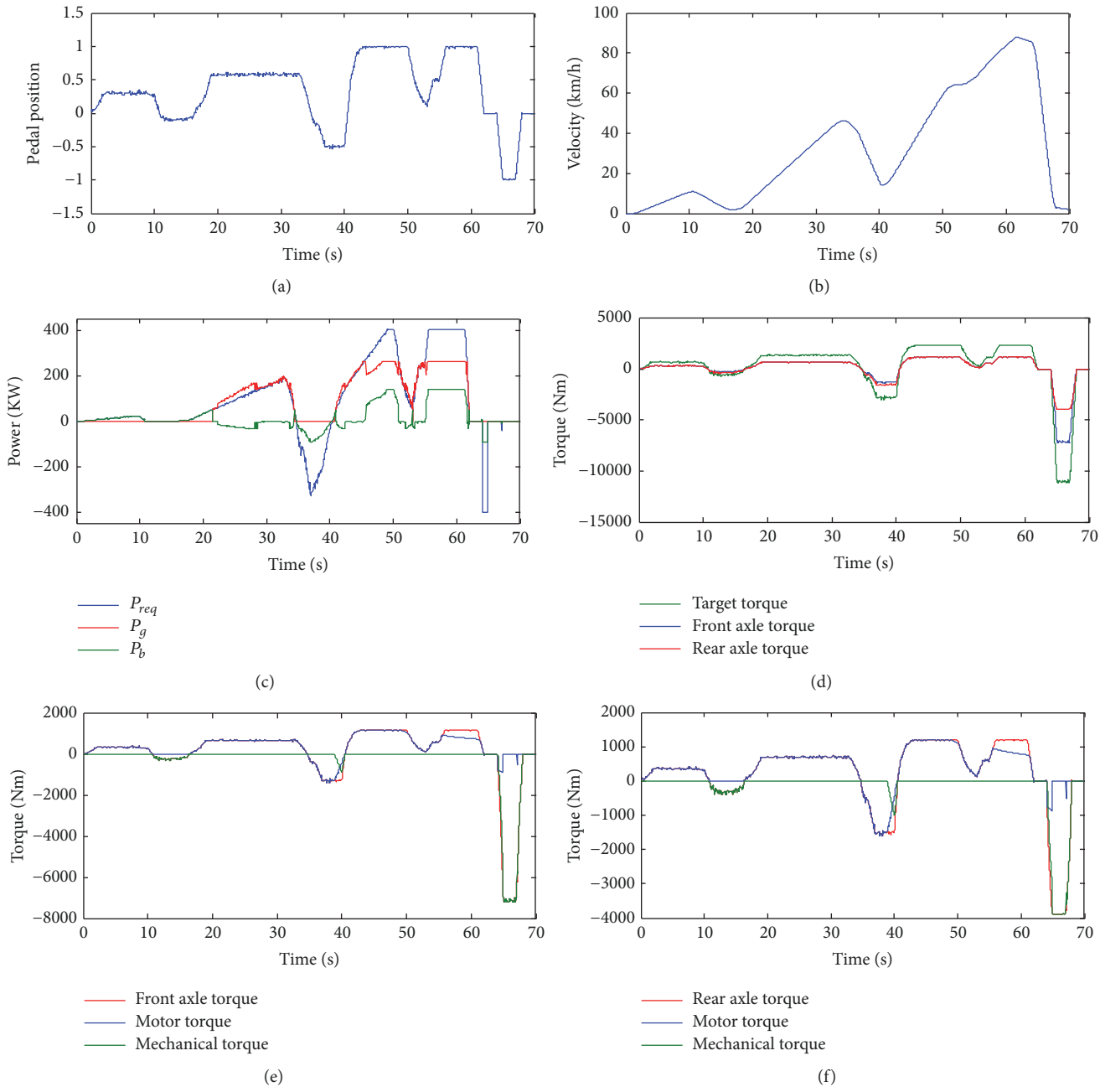

FIGURE 21: The results of HILS experiment.

to be analyzed in different situations. In 12-17s, because the speed is lower than 12 km/h, only mechanical braking is carried out. In 34-38s, the braking strength is less than 0.7, and the require torque is smaller than the maximum braking torque of motor, so only regenerative braking is carried out. In 39-41s, the speed is reduced from 24 km/h to 14 km/h, so the regenerative braking torque gradually becomes smaller and the mechanical braking torque gradually becomes larger. In 66-68s, the vehicle is in an emergency braking state, and the braking strength is more than 0.7, so the braking torque is totally provided by the mechanical brake.

6. Conclusions

In this paper, an energy management strategy combining fuzzy control and threshold control was proposed for a series hybrid electric rescue vehicle, and a FLC optimization method based on IQGA was introduced to further improve the fuel economy. The effectiveness and real-time performance of the proposed EMS were validated by simulation and HILS experiment. The simulation results show that, compared with QGA and GA, the IQGA optimization algorithm has faster convergence speed and better optimization

result. With IQGA optimization EMS, the engine efficiency is obviously improved, and the fuel consumption can be reduced by 5.17% compared with that before optimization. The HILS experiment shows that, with the proposed EMS, the real-time requirements of the vehicle can be well satisfied, the working characteristics of IGPU and battery can be effectively exploited, and the braking energy can be fully absorbed by the front and rear motor. In conclusion, the EMS proposed in this paper has achieved good control effect, which can be used in real-time control of the series hybrid electric rescue vehicle.

Data Availability

The data used to support the findings of this study are available from the corresponding author upon request.

Conflicts of Interest

The authors declare that there are no conflicts of interest regarding the publication of this paper.

Acknowledgments

This work was financially supported by National Key R&D Program of China (2016YFC0802900).

References

[1] K. Ç. Bayindir, M. A. Gözüküçük, and A. Teke, "A comprehensive overview of hybrid electric vehicle: powertrain configurations, powertrain control techniques and electronic control units," *Energy Conversion and Management*, vol. 52, no. 2, pp. 1305–1313, 2011.

[2] Ehsani. Mehrdad, Gao. Yimin, and Ali. Emadi, *Modern Electric, Hybrid Electric, And Fuel Cell Vehicles : Fundamentals, Theory, And Design*, CRC Press, Boca Raton, Fl, USA, 2009.

[3] C. Dextreit and I. V. Kolmanovsky, "Game theory controller for hybrid electric vehicles," *IEEE Transactions on Control Systems Technology*, vol. 22, no. 2, pp. 653–663, 2014.

[4] H. Banvait, S. Anwar, and Y. Chen, "A rule-based energy management strategy for Plugin Hybrid Electric Vehicle (PHEV)," in *Proceedings of the American Control Conference (ACC '09)*, pp. 3938–3943, St. Louis, Mo, USA, June 2009.

[5] X. Wang, H. He, F. Sun, and J. Zhang, "Application study on the dynamic programming algorithm for energy management of plug-in hybrid electric vehicles," *Energies*, vol. 8, no. 4, pp. 3225–3244, 2015.

[6] B. C. Chen, Y. Y. Wu, and H. C. Tsai, "Design and analysis of power management strategy for range extended electric vehicle using dynamic programming," *Applied Energy*, vol. 113, pp. 1764–1774, 2014.

[7] C. Hou, M. Ouyang, L. Xu, and H. Wang, "Approximate Pontryagin's minimum principle applied to the energy management of plug-in hybrid electric vehicles," *Applied Energy*, vol. 115, pp. 174–189, 2014.

[8] S. Zhang, R. Xiong, and C. Zhang, "Pontryagin's Minimum Principle-based power management of a dual-motor-driven electric bus," *Applied Energy*, vol. 159, pp. 370–380, 2015.

[9] Z. Zhou and C. Mi, "Power management of PHEV using quadratic programming," *International Journal of Electric and Hybrid Vehicles*, vol. 3, no. 3, pp. 246–258, 2011.

[10] Z. Chen, C. C. Mi, R. Xiong, J. Xu, and C. You, "Energy management of a power-split plug-in hybrid electric vehicle based on genetic algorithm and quadratic programming," *Journal of Power Sources*, vol. 248, pp. 416–426, 2014.

[11] Z. Yarning, S. Fengchun, and H. Hongwen, "Control strategy optimization for hybrid electric vehicle based on DIRECT algorithm," in *Proceedings of the 2008 IEEE Vehicle Power and Propulsion Conference, VPPC 2008*, China, September 2008.

[12] A. Panday and H. O. Bansal, "Fuel efficiency optimization of input-split hybrid electric vehicle using DIRECT algorithm," in *Proceedings of the 9th IEEE International Conference on Industrial and Information Systems, ICIIS 2014*, India, December 2014.

[13] J. Hao, Z. Yu, Z. Zhao, P. Shen, and X. Zhan, "Optimization of key parameters of energy management strategy for hybrid electric vehicle using DIRECT algorithm," *Energies*, vol. 9, no. 12, 2016.

[14] P. Elbert, T. Nuesch, A. Ritter, N. Murgovski, and L. Guzzella, "Engine on/off control for the energy management of a serial hybrid electric bus via convex optimization," *IEEE Transactions on Vehicular Technology*, vol. 63, no. 8, pp. 3549–3559, 2014.

[15] J. Park and J.-H. Park, "Development of equivalent fuel consumption minimization strategy for hybrid electric vehicles," *International Journal of Automotive Technology*, vol. 13, no. 5, pp. 835–843, 2012.

[16] T. Nüesch, A. Cerofolini, and G. Mancini, "Equivalent consumption minimization strategy for the control of real driving NOx emissions of a diesel hybrid electric vehicle," *Energies*, vol. 7, no. 5, pp. 3148–3178, 2014.

[17] G. Paganelli, T. M. Guerra, S. Delprat, J. J. Santin, M. Delhom, and E. Combes, "Simulation and assessment of power control strategies for a parallel hybrid car," *Proceedings of the Institution of Mechanical Engineers, Part D: Journal of Automobile Engineering*, vol. 214, no. 7, pp. 705–718, 2000.

[18] K. Yu, H. Yang, X. Tan et al., "Model Predictive Control for Hybrid Electric Vehicle Platooning Using Slope Information," *IEEE Transactions on Intelligent Transportation Systems*, vol. 17, no. 7, pp. 1894–1909, 2016.

[19] X. Zeng and J. Wang, "A Parallel Hybrid Electric Vehicle Energy Management Strategy Using Stochastic Model Predictive Control With Road Grade Preview," *IEEE Transactions on Control Systems Technology*, vol. 23, no. 6, pp. 2416–2423, 2015.

[20] V. T. Minh and A. A. Rashid, "Modeling and model predictive control for hybrid electric vehicles," *International Journal of Automotive Technology*, vol. 13, no. 3, pp. 477–485, 2012.

[21] K. M. Passino and S. Yurkovich, "Fuzzy Control," in *The Control Systems Handbook*, CRC Press, 2001.

[22] L. Wang, "Stable adaptive fuzzy control of nonlinear systems," *IEEE Transactions on Fuzzy Systems*, vol. 1, no. 2, pp. 146–155, 1993.

[23] S. G. Li, S. M. Sharkh, F. C. Walsh, and C. N. Zhang, "Energy and battery management of a plug-in series hybrid electric vehicle using fuzzy logic," *IEEE Transactions on Vehicular Technology*, vol. 60, no. 8, pp. 3571–3585, 2011.

[24] H. Hannoun, D. Diallo, and C. Marchand, "Energy management strategy for a parallel hybrid electric vehicle using fuzzy logic," in *Proceedings of the International Symposium on Power Electronics, Electrical Drives, Automation and Motion, 2006. SPEEDAM 2006*, pp. 230–234, Italy, May 2006.

[25] A. S. Sarvestani and A. A. Safavi, "A novel optimal energy management strategy based on fuzzy logic for a hybrid electric vehicle," in *Proceedings of the 2009 IEEE International Conference on Vehicular Electronics and Safety, ICVES 2009*, pp. 141–145, India, November 2009.

[26] D. Zhao, R. Stobart, G. Dong, and E. Winward, "Real-Time Energy Management for Diesel Heavy Duty Hybrid Electric Vehicles," *IEEE Transactions on Control Systems Technology*, vol. 23, no. 3, pp. 829–841, 2015.

[27] Y. Yang, P. Ye, X. Hu, B. Pu, L. Hong, and K. Zhang, "A research on the fuzzy control strategy for a speed-coupling ISG HEV based on dynamic programming optimization," *Qiche Gongcheng/Automotive Engineering*, vol. 38, no. 6, pp. 674–679, 2016.

[28] A. Poursamad and M. Montazeri, "Design of genetic-fuzzy control strategy for parallel hybrid electric vehicles," *Control Engineering Practice*, vol. 16, no. 7, pp. 861–873, 2008.

[29] J. Liang, J. Zhang, H. Zhang, and C. Yin, "Fuzzy energy management optimization for a parallel hybrid electric vehicle using chaotic non-dominated sorting genetic algorithm," *Automatika – Journal for Control, Measurement, Electronics, Computing and Communications*, vol. 56, no. 2, pp. 149–163, 2015.

[30] J. Wu, C.-H. Zhang, and N.-X. Cui, "Fuzzy energy management strategy for a hybrid electric vehicle based on driving cycle recognition," *International Journal of Automotive Technology*, vol. 13, no. 7, pp. 1159–1167, 2012.

[31] N. Limin, H. Yang, and Y. Zhang, "Intelligent HEV Fuzzy Logic Control Strategy Based on Identification and Prediction of Drive Cycle and Driving Trend," *World Journal of Engineering & Technology*, vol. 3, no. 3, pp. 215–226, 2015.

[32] Y. L. Murphey, Z. Chen, L. Kiliaris, and M. A. Masrur, "Intelligent power management in a vehicular system with multiple power sources," *Journal of Power Sources*, vol. 196, no. 2, pp. 835–846, 2011.

[33] R. Langari and J.-S. Won, "Intelligent energy management agent for a parallel hybrid vehicle—part I: system architecture and design of the driving situation identification process," *IEEE Transactions on Vehicular Technology*, vol. 54, no. 3, pp. 925–934, 2005.

[34] K. H. Han and J. H. Kim, "Genetic quantum algorithm and its application to combinatorial optimization problem," in *Proceedings of the IEEE International Conference on Evolutionary Computation*, pp. 1354–1360, San Diego, Calif, USA, July 2000.

[35] S. Borthakur and S. C. Subramanian, "Parameter matching and optimization of a series hybrid electric vehicle powertrain system," in *Proceedings of the ASME 2016 International Mechanical Engineering Congress and Exposition, IMECE 2016*, USA, November 2016.

[36] Q. Tu, X. Zhang, M. Pan, C. Jiang, and J. Xue, "Design and Optimization of the Power Management Strategy of an Electric Drive Tracked Vehicle," *Mathematical Problems in Engineering*, vol. 2016, Article ID 6185743, 13 pages, 2016.

[37] K. Wipke, T Keith, and D. Nelson, "Optimizing Energy Management Strategy and Degree of Hybridization for a Hydrogen Fuel Cell SUV," https://www.researchgate.net/publication/2868610_Optimizing_Energy_Management_Strategy_and_Degree_of_Hybridization_for_a_Hydrogen_Fuel_Cell_SUV.

[38] T. A. T. Mohd, M. K. Hassan, I. Aris, C. S. Azura, and B. S. K. K. Ibrahim, "Application of fuzzy logic in multi-mode driving for a battery electric vehicle energy management," *International Journal on Advanced Science, Engineering and Information Technology*, vol. 7, no. 1, pp. 284–290, 2017.

[39] F. Sun and C. Zhang, *Technoloyies for the hybrid electric drive system of armored vehicle*, National Defense Industry Press, 2017.

[40] H. W. He, R. Xiong, H. Q. Guo, and S. C. Li, "Comparison study on the battery models used for the energy management of batteries in electric vehicles," *Energy Conversion and Management*, vol. 64, pp. 113–121, 2012.

[41] W. Waag, C. Fleischer, and D. U. Sauer, "On-line estimation of lithium-ion battery impedance parameters using a novel varied-parameters approach," *Journal of Power Sources*, vol. 237, pp. 260–269, 2013.

[42] K. Meah, S. Hietpas, and S. Ula, "Rapid control prototyping of a permanent magnet DC motor drive system using dSPACE and mathworks simulink," in *Proceedings of the APEC 2007 - 22nd Annual IEEE Applied Power Electronics Conference and Exposition*, pp. 856–861, USA, March 2007.

[43] A. Rubaai and P. Young, "Hardware/software implementation of fuzzy-neural-network self-learning control methods for brushless DC motor drives," *IEEE Transactions on Industry Applications*, vol. 52, no. 1, pp. 414–424, 2016.